

Retrospective Memory for Camouflaged Object Detection

Chenxi Zhang
zhangchenxi2025@163.com
Shanghai Institute of Technology
Shanghai, China

Jiayun Wu
wujiayun_110@163.com
Shanghai Institute of Technology
Shanghai, China

Qing Zhang*
zhangqing@sit.edu.cn
Shanghai Institute of Technology
Shanghai, China

Yazhe Zhai
zhaiyazhe@njust.edu.cn
Nanjing University of Science
Nanjing, China

Youwei Pang*
lartpang@gmail.com
Dalian University of Technology
Dalian, China

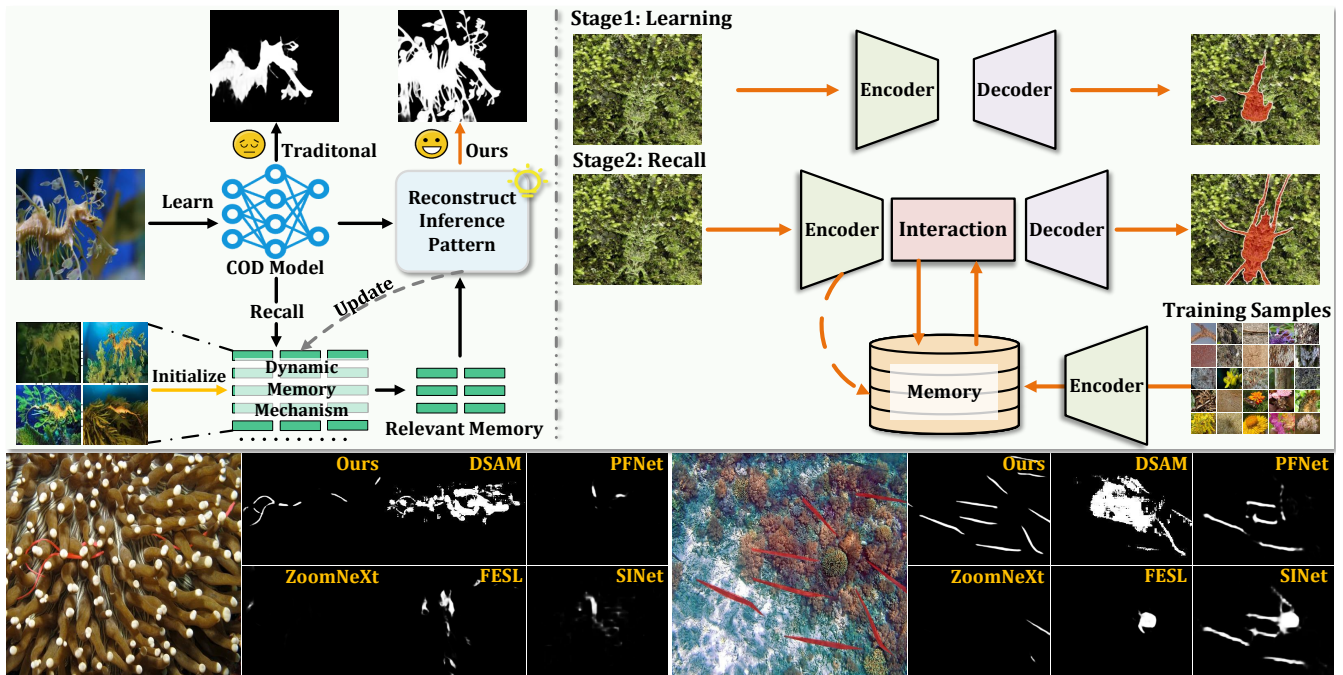


Figure 1: *Left*: Overview of the proposed method, featuring a dynamic memory mechanism for learned knowledge recall and memory representation updating to handle challenging camouflage cases more effectively. *Right*: Two-stage pipeline of our method consisting of learning and recall stages. *Bottom*: Visual comparison with SOTA methods in challenging camouflage scenes, e.g., cluttered backgrounds (*left*) and multiple objects (*right*), showcasing our model’s superior robustness.

Abstract

Camouflaged object detection (COD) primarily focuses on learning subtle yet discriminative representations from complex scenes. Existing methods predominantly follow the parametric feedforward architecture based on static visual representation modeling. However, they lack explicit mechanisms for acquiring historical context, limiting their adaptation and effectiveness in handling challenging camouflage scenes. In this paper, we propose a recall-augmented COD architecture, *i.e.*, **RetroMem**, which dynamically modulates camouflage pattern perception and inference by integrating relevant historical knowledge into the process. Specifically, RetroMem employs a two-stage training paradigm consisting of a learning stage and a recall stage to construct, update, and utilize memory

representations effectively. During the learning stage, we design a dense multi-scale adapter (DMA) to improve the pretrained encoder’s capability to capture rich multi-scale visual information with very few trainable parameters, thereby providing foundational inferences. In the recall stage, we propose a dynamic memory mechanism (DMM) and an inference pattern reconstruction (IPR). These components fully leverage the latent relationships between learned knowledge and current sample context to reconstruct the inference of camouflage patterns, thereby significantly improving the model’s understanding of camouflage scenes. Extensive experiments on several widely used datasets demonstrate that our RetroMem significantly outperforms existing state-of-the-art methods.

*Corresponding author

1 Introduction

In nature, many animals adopt sophisticated camouflage patterns to interfere with predators' visual perception, thereby effectively concealing themselves within their environments. The core of the camouflaged object detection (COD) task is to accurately segment these concealed objects from scenes that exhibit high visual similarity between targets and backgrounds. Nevertheless, the inherent diversity of camouflage patterns and the complexity of real-world scenes significantly increase the difficulty of this task. Due to its practical significance, COD research has been broadly applied across various domains, including wildlife protection [41], medical image analysis [14], and agricultural monitoring [51].

Early COD methods rely on handcrafted features, such as texture [53], motion flow [21] and color contrast [48]. These pioneering methods, however, suffer from inherent limitations in robustness and flexibility, restricting their applicability to diverse and complex visual scenes. Recent advances in deep learning have substantially driven the COD field including attention mechanisms [56, 65, 67], bio-inspired perception [44, 45], and multi-task joint frameworks [18, 55] to extract subtle yet critical visual cues and construct multi-scale/view joint feature modeling for camouflage scene understanding. Despite notable improvements, existing methods remain fundamentally constrained by their architectural paradigms. The prevailing approach excessively prioritizes the design of sequentially stacked modules for progressive feature refinement, while adhering to static inference patterns reliant on instantaneous visual cues. This dual focus however neglects the systematic integration of historical contextual knowledge and fails to enable effective reuse of acquired representational capabilities during network learning. Consequently, these architectures exhibit critical deficiencies in dynamic adaptability and responsive mechanism design. These constraints impair their performance to handle challenging camouflage scenes with diverse object characteristics and environmental conditions. Targeted benchmark evaluations on unseen/rare scenes (Tab. 6) reveal significant performance degradation in more challenging cases. The results expose existing architectural limitations in scene adaptability. These findings necessitate the COD framework design capable of synergizing historical contextual knowledge with adaptive inference pattern reconstruction. This approach enables the context-aware inference mechanism to achieve robust cross-scene generalization.

Inspired by the above discussion, we propose **RetroMem** (Fig. 1 *Left*), a novel COD paradigm inspired by the human brain's recall mechanism [58]. This framework simulates human-like adaptive inference through dynamically reconstructing inference pattern. It injects historical knowledge into the current observation, which moves beyond static feature reliance to enhance generalization in complex camouflage scenes (Fig. 1 *Bottom*). Grounded in the Confucian principle "*Learn from the past and understand the present*" (Fig. 1 *Right*), RetroMem implements a **two-stage training framework** for strategic knowledge integration. The initial **learning stage** deploys the dense multi-scale adapter (DMA) to finetune DINOv2 [43]-based visual encoding. This establishes foundational perception and segmentation capabilities for camouflaged objects. The subsequent **recall stage** addresses architectural limitations by further introducing a learnable dynamic memory bank. It stores

and updates acquired knowledge during training, and enables adaptive recall of semantic-relevant representations during inference. Considering knowledge transfer challenges from camouflage pattern variations between historical and current samples, we develop an inference pattern reconstruction (IPR). It dynamically synthesizes memory-derived historical insights with current visual evidence, significantly boosting adaptive inference capacity. Specifically, RetroMem initially employs the segmentation capability acquired during the learning stage to identify subtle visual indicators suggestive of camouflaged objects. It then recalls the most relevant prototype representations from the memory bank as historical context. Finally, the IPR module integrates these components to reconstruct specific inference patterns for current samples. Such a design improves the model performance in diverse camouflage challenges through context-aware decision-making.

Our main contributions are summarized as follows:

- We propose **RetroMem**, a two-stage training framework designed to reconstruct the architectural paradigm for COD, mitigating the reliance on the instantaneous visual cues and the static inference pattern in conventional designs.
- We introduce the dense multi-scale adapter to effectively fine-tune the visual encoder for high-performance COD.
- We design a learnable dynamic memory mechanism (DMM) that efficiently stores and updates the contextual memory, enabling adaptive knowledge recall.
- We propose the inference pattern reconstruction to inject the recalled knowledge, which dynamically improves the sample-specific visual inference.
- Experiments on multiple conventional and carefully-constructed challenging COD benchmarks demonstrate the effectiveness and generalization of RetroMem.

2 Related Work

2.1 Camouflaged Object Detection (COD)

Camouflage scenes are characterized by subtle visual cues that are frequently imperceptible to human observers. However, these cues encapsulate critical contextual information exposing latent patterns in visual data. The fundamental objective of COD resides in extracting these concealed yet discriminative features within intricate environments, thereby enabling accurate detection of camouflaged objects and recovery of their intrinsic structural characteristics.

Recent years have seen rapid progress in COD research, driven by novel approaches that enhance scene understanding through advanced perception mechanisms. Biologically-inspired methods demonstrate particular efficacy. The two-stage search-and-recognition processes are adopted in [13, 40] to first localize and then segment objects with increasing precision. Some works [44, 45] employ dynamic multi-scale integration to resolve semantic relationships between ambiguous objects and their contexts. Concurrently, multi-task paradigms improve object discernment by jointly optimizing auxiliary tasks like edge detection [26, 35, 55]. Spectral processing techniques [18, 56] are also introduced to integrate global representation and extract discriminative details in the frequency domain, effectively amplifying subtle camouflage patterns. Additionally, several methods [65, 67] explore intrinsic foreground-background interactions for more robust segmentation. Beyond the

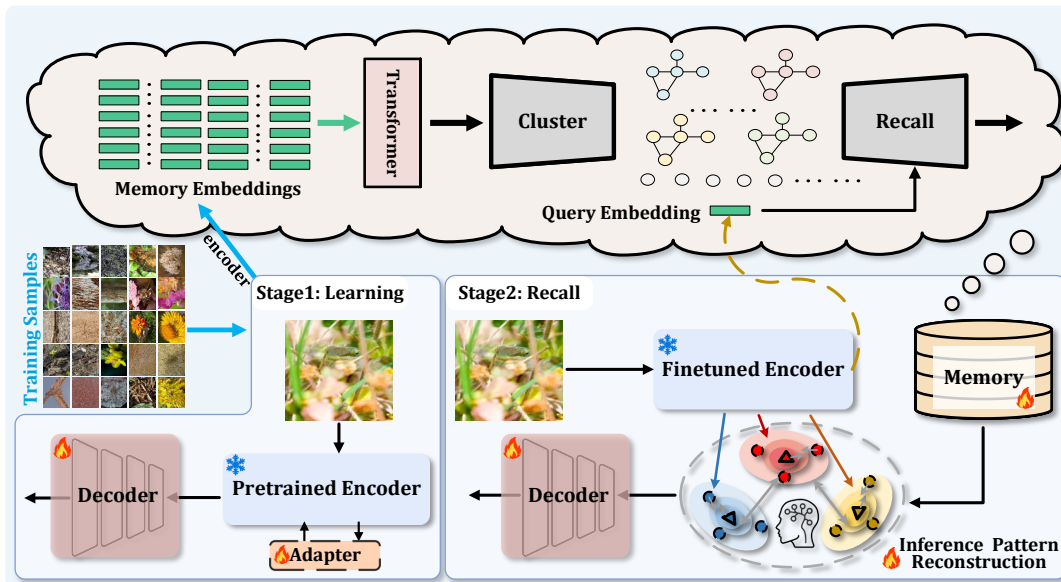


Figure 2: Overview of the proposed RetroMem based on a two-stage training paradigm. The learning stage constructs a conventional COD network with multi-scale dense adapters to efficiently fine-tune the pretrained encoder, while embedding the training set into the memory. During the recall stage, specific inference patterns are dynamically reconstructed through recall of relevant memory embeddings for each input sample.

aforementioned RGB-centric methods, emerging COD methods explore cross-modal synergies through complementary semantic integration. Representative implementations include geometric-aware frameworks [60, 66] that leverage depth-derived structural priors to resolve spatial ambiguities, and vision-language paradigms [68, 69] that incorporate textual descriptors to establish semantic correspondences with camouflaged object representations. Despite these advances, current COD methods remain hampered by their reliance on the instantaneous visual cues and the sample-common inference mechanism, struggling in complex scenes (Fig. 1 *Bottom*). Like students excelling in drills but failing in practice, they perform well on test samples that mirror training data but falter under challenging scenes (e.g., rare, unseen camouflage scenes as discussed in Sec. 4.3 and Tab. 6). This demands an adaptive mechanism that integrates learned knowledge with runtime contextual inference.

2.2 Memory Mechanism

The concept of memory is deeply rooted in human cognition, enabling individuals to store and recall past experiences to guide future perception and decision-making [1, 17, 31]. Inspired by this biological foundation, memory mechanisms have been incorporated into artificial intelligence systems, enabling models to retain and reuse informative representations over time. In deep learning, the Long Short-Term Memory (LSTM) network [20] is among the earliest architectures to explicitly introduce memory into neural networks, effectively capturing long-range dependencies in sequential data. Building on this foundation, memory mechanisms have been widely adopted in tasks like video segmentation and anomaly detection, aiming to establish stable reference representations to enhance object region discrimination. In video segmentation, models

such as XMem [5] and RMem [42] mimic human sensory memory through multi-level memory hierarchies and attention-based retrieval, facilitating robust long-term tracking. Others, including CUTIE [63] and CompFeat [34], shift from pixel-level to object-level memory representations to achieve better generalization, while some approaches [59] use dynamic memory updates to retain only essential information. In anomaly detection, early methods based on autoencoders relied on reconstruction errors but often suffered from overfitting, limiting anomaly discrimination. MemAE [16] addressed this by incorporating an external memory module with attention-based retrieval to reconstruct inputs using prototypical normal features. More recent patch-level methods, such as PatchCore [50] and SoftPatch [27], construct non-parametric memory banks from local features and employ KNN [7] for improved anomaly localization. TailedCore [28] further enhances robustness by selectively retaining rare-class features and applying noise filtering to achieve a balanced memory bank. Unlike anomaly detection and video segmentation, which rely on stable reference patterns such as normality in appearance or temporal consistency across frames, COD is a *class-agnostic* task in which the model is required to handle previously unseen object categories during inference. And camouflaged object lacks both clear semantic structure and salient visual cues. These characteristics limit the effectiveness of conventional memory-based approaches. To address these limitations, we propose a dynamic memory mechanism specifically tailored for COD. Instead of relying on fixed or temporally aligned references, our method constructs a memory bank from diverse training samples. During inference, the model recalls semantically similar memory based on input features, providing essential contextual cues to accurately identify camouflaged objects.

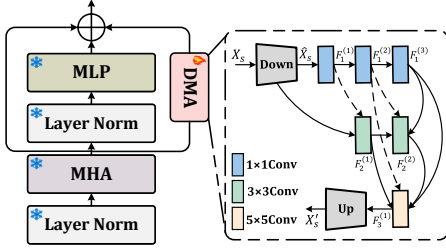


Figure 3: Illustration of the dense multi-scale adapter (DMA).

3 Methodology

3.1 Overall Architecture

As depicted in Fig. 2, the proposed RetroMem framework combines two synergistic stages. The learning stage constructs a simple conventional COD model to encode all training samples into high-level features, forming an initialized memory bank. During the recall stage, the framework dynamically recalls the most semantically relevant prototype from this bank for each input sample, aligns its visual features through the inference pattern reconstruction, and processes the reconstructed feature flow via the decoder to generate segmentation results. Notably, the memory bank undergoes iterative improvement during recall-stage training by clustering semantically similar embeddings, which progressively enhances the stored representations to encapsulate discriminative knowledge. This closed-loop architecture enables simultaneous feature preservation and adaptive inference pattern adjustment.

3.2 Stage 1: Learning

In the learning stage, our COD model consists of a DINOv2 [43]-based encoder and a simple multi-scale feature decoder. Given an input image $X_I \in \mathbb{R}^{H \times W \times 3}$, we first extract multi-scale features $\{F_i\}_{i=1}^3$ from the encoder, and then progressively integrate them to obtain the camouflaged object prediction in the decoder.

Dense Multi-scale Adapter (DMA). Although DINOv2 [43] shows strong transfer learning performance across various downstream vision tasks, the conventional full finetuning strategy may yield suboptimal results in the COD task, as shown in [supplementary material](#) (Sec. B.4). This stems from the tension between the massive trainable parameters in DINOv2 and the relatively limited training data in COD, creating high risks of overfitting. Furthermore, while multi-scale information integration is known to be critical for COD [44, 45], naively finetuning all layers fails to explicitly exploit such inductive biases. To this end, we propose the DMA shown in Fig. 3 to transform the pretrained DINOv2 into a COD specialist via lightweight architectural adaptation. By injecting trainable dense fusion paths in the frozen backbone, the DMA preserves DINOv2’s generalizable visual representations by freezing original parameters and enables context-aware aggregation of cross-scale features for precise camouflage object perception. Specifically, our DMA first utilizes a linear projection layer ($Linear_{\text{down}}$) to reduce the dimension of the input feature X_s :

$$\hat{X}_s = \sigma(\text{Linear}_{\text{down}}(X_s)) \quad (1)$$

where σ is the non-linear activation function, *i.e.*, ReLU. Then, we use three 1×1 convolutional layers to generate features $\{F_1^{(n)}\}_{n=1}^3$:

$$F_1^{(n)} = \begin{cases} \text{Conv}_{1 \times 1}(\hat{X}_s) & \text{if } n = 1 \\ \text{Conv}_{1 \times 1}(F_1^{(n-1)}) & \text{if } n = 2, 3 \end{cases} \quad (2)$$

where $\text{Conv}_{k \times k}$ represents the convolution layer with a kernel size of k . Next, mid-scale context representation $\{F_2^{(n)}\}_{n=1}^2$ is extracted by 3×3 convolution layers and integrated with $F_1^{(n)}$ to enhance structural details:

$$F_2^{(1)} = \text{Conv}_{3 \times 3}(\text{Conv}_{1 \times 1}([\hat{X}_s, F_1^{(1)}])) \quad (3)$$

$$F_2^{(2)} = \text{Conv}_{3 \times 3}(\text{Conv}_{1 \times 1}([F_2^{(1)}, F_1^{(2)}, F_1^{(3)}])) \quad (4)$$

where $[\cdot]$ denotes the channel-wise concatenation operation. Additionally, a 5×5 convolutional layer aggregates these features to capture information across different receptive fields, thus effectively discriminating local details:

$$F_3^{(1)} = \text{Conv}_{5 \times 5}(\text{Conv}_{1 \times 1}([F_2^{(1)}, F_2^{(2)}, F_1^{(2)}, F_1^{(3)}])) \quad (5)$$

The final output X'_s of the DMA is obtained via a linear up-projection layer $Linear_{\text{up}}$ which restores the original channel dimension:

$$X'_s = \text{Linear}_{\text{up}}(F_3^{(1)}) \quad (6)$$

Instead of merely combining multi-scale features, our DMA hierarchically aggregates localized patterns across varying scales through dense connections, ensuring progressive refinement while preserving fine-grained details.

3.3 Stage 2: Recall

This stage aims to alleviate the generalization bottleneck of the model through the learnable dynamic memory coupled with adaptive inference pattern reconstruction, enabling dual adaptation to diverse camouflage scenes. Initially, feature embeddings from training samples are adaptively clustered into a prototype memory bank \mathcal{M} that encodes representative prototypes of various camouflage patterns. Multi-level features $\{F_i\}_{i=1}^3$ extracted by the frozen encoder drive cosine similarity-based retrieval of the most relevant prototype \hat{p}_q from \mathcal{M} , with the deepest feature F_3 serving as the query embedding. This retrieved representation triggers sample-specific pattern reconstruction through semantic attribute clustering to dynamically align the historical context with current features. The mechanism preserves fidelity to learned camouflage patterns via memory-based recall while achieving the adaptation to diverse scenes through the online-updated inference pattern.

Dynamic Memory Mechanism (DMM). The memory bank \mathcal{M} is initialized by processing all N training images through the Stage 1-finetuned encoder, where ℓ_2 -normalized and globally average-pooled features form preliminary embeddings $M \in \mathbb{R}^{N \times C}$. These embeddings are enhanced as $M_e \in \mathbb{R}^{N \times C}$ through a single transformer layer [57]. M_e is subsequently assigned to their respective clusters and converted to $M_c \in \mathbb{R}^{N \times C}$ by HDBSCAN [39], which adaptively groups similar embeddings into K^1 semantically distinctive clusters with center prototypes $P_c = \{p_k\}_{k=1}^K$. This process not only mitigates computational redundancy and noisy interferences from raw

¹Due to the nature of HDBSCAN, K does not need to be specified manually.

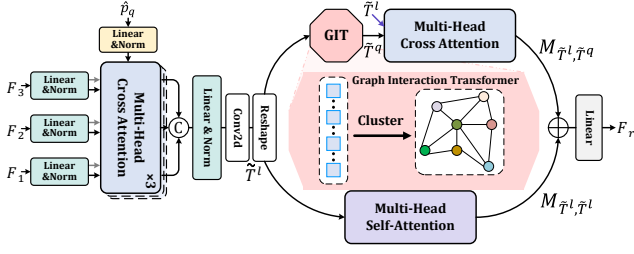


Figure 4: Illustration of the inference pattern reconstruction.

sample-level storage and recall, but also captures shared semantic characteristics among different camouflage instances. During training, we iteratively optimize the transformer parameters and update the memory bank by constraining the consistency of the representation M_e with the clustered memory prototypes as detailed in Sec. 3.5. By this way, the memory bank can be refined into a compact and discriminative form. Next, the cosine distance is used to determine the sample-prototype similarity for the query embedding f_q from the deepest layer in the encoder:

$$s_{q,k} = \frac{\langle f_q, p_k \rangle}{\|f_q\|_2 \|p_k\|_2}, \quad k = 1, 2, \dots, K \quad (7)$$

where $\langle \cdot, \cdot \rangle$ and $\|\cdot\|_2$ are the inner product between vectors and the ℓ_2 norm, respectively. And the most relevant prototype is:

$$\hat{p}_q = P_c [\arg \max_k s_{q,k}] \in R^C \quad (8)$$

The final prototype \hat{p}_q is used to adjust and reconstruct the forward propagation of the multi-level encoder features.

Inference Pattern Reconstruction (IPR). The recalled memory prototype \hat{p}_q serves as a condensed and semantically rich representation of a cluster of camouflage patterns, offering valuable inference context. So, we introduce the IPR shown in Fig. 4 to integrate \hat{p}_q in a context-aware manner. By establishing multi-dimensional correlations across these heterogeneous feature sources, it enables robust and adaptive inference across diverse camouflage scenes. The IPR employs a multi-step feature interaction strategy to integrate the memory embedding \hat{p}_q and multi-level visual features at multiple scales, enhancing hidden correlations in latent dimensions. We first introduce multi-head cross-attention [57] to compute their correlations. Given the embedding \hat{p}_q and multi-level encoder features $\{F_i\}_{i=1}^3$, the query F_i^q , key T^k and value T^v are computed by the projection matrices W_q , W_k and W_v :

$$F_i^q = \text{reshape}(F_i)W_q \in \mathbb{R}^{H_i W_i \times C^l}, \quad i \in \{1, 2, 3\} \quad (9)$$

$$T^k = \text{reshape}(\hat{p}_q)W_k, T^v = \text{reshape}(\hat{p}_q)W_v \in \mathbb{R}^{1 \times C^l}, \quad (10)$$

$$T_i^l = \text{Softmax} \left(\frac{F_i^q (T^k)^\top}{\sqrt{C^l}} \right) T^v \in \mathbb{R}^{H_i W_i \times C^l} \quad (11)$$

where C^l is the channel number of F_i^q , T^k and T^v . To further enhance semantic expression, the refined feature \tilde{T}^l is first projected into a latent graph space, where similar semantic features are clustered into graph nodes. And then, we introduce the graph interaction transformer (GIT) [64] in IPR to aggregate these features as \tilde{T}^q ,

which serves as a structured representation capturing long-range contextual information. By leveraging graph-based clustering, the GIT ensures that similar camouflage patterns are represented in a compact and consistent manner, facilitating robust inference across complex scenes. Then, the cross-attention between \tilde{T}^q and \tilde{T}^l and the self-attention of \tilde{T}^l aggregate and reconstruct the inference pattern, yielding the final enhanced feature F_r :

$$M_{\tilde{T}^l \leftarrow \tilde{T}^q} = \text{Softmax} \left(\frac{W_q \tilde{T}^q (W_k \tilde{T}^l)^\top}{\sqrt{C^l}} \right) W_v \tilde{T}^l \quad (12)$$

$$F_r = M_{\tilde{T}^l, \tilde{T}^l} + M_{\tilde{T}^l, \tilde{T}^q} \quad (13)$$

where \tilde{T}^o denotes either \tilde{T}^q or \tilde{T}^l . The output feature F_r serves as guidance for subsequent inference. Rather than relying solely on the feature similarity, our IPR adaptively models contextual consistency and constructs the sample-specific inference process by integrating the current representation with the semantic-relevant memory prototype. It enables the model generalization across diverse camouflage scenes by aligning and combining historical knowledge with the current input, thereby enhancing accuracy and robustness.

3.4 Decoder Network

To effectively utilize the inference guidance F_r , we design a simple yet efficient decoder. We employ the convolutional LSTM (Γ) to progressively fuse multi-level features $\{\tilde{F}_i\}_{i=1}^3$, where F_r serves as a long-term memory item:

$$\tilde{F}_i = \begin{cases} \Gamma(F_3, F_3) + F_3 & \text{if } i = 3 \\ \Gamma(F_i, [\text{Up}(\tilde{F}_{i+1}), \text{Up}(F_3)]) + \text{Up}(\tilde{F}_{i+1}) & \text{if } i = 2, 1 \text{ in Sec. 3.2} \\ \Gamma(F_i, [\text{Up}(\tilde{F}_{i+1}), \text{Up}(F_r)]) + \text{Up}(\tilde{F}_{i+1}) & \text{if } i = 2, 1 \text{ in Sec. 3.3} \end{cases} \quad (14)$$

where “Up” is the bilinear interpolation for spatial alignment. Finally, the 1×1 convolution is applied to reduce the channel dimension and produce the segmentation predictions $\{P_i\}_{i=1}^3$ from features $\{\tilde{F}_i\}_{i=1}^3$, respectively.

3.5 Loss Function

Following existing COD methods [45, 60], we adopt a hybrid loss ($\mathcal{L}_{\text{seg}} = \mathcal{L}_{\text{bce}} + \mathcal{L}_{\text{iou}}$) consisting of the binary cross-entropy loss (\mathcal{L}_{bce}) and the IoU loss (\mathcal{L}_{iou}) during training. This hybrid loss provides a good balance between pixel-wise accuracy and region-level consistency. Besides, we introduce a consistency loss \mathcal{L}_c , which encourages the transformer in our memory to form structurally and semantically consistent feature spaces with the clustering results by minimizing the distance between the each instant $M_e[i] \in \mathbb{R}^C$ and its corresponding cluster prototype $M_c[i] \in \mathbb{R}^C$:

$$\mathcal{L}_c(M_e, M_c) = \frac{1}{N} \sum_{i=1}^N \|M_e[i] - M_c[i]\|_2^2 \quad (15)$$

where the embeddings $M_e, M_c \in \mathbb{R}^{N \times C}$ are from the transformer layer and the clustering algorithm as described in Sec. 3.3, respectively. So, our overall loss function is defined as:

$$\mathcal{L} = \sum_{i=1}^3 \mathcal{L}_{\text{seg}}(P_i, G) + \mathcal{L}_c(M_e, M_c) \quad (16)$$

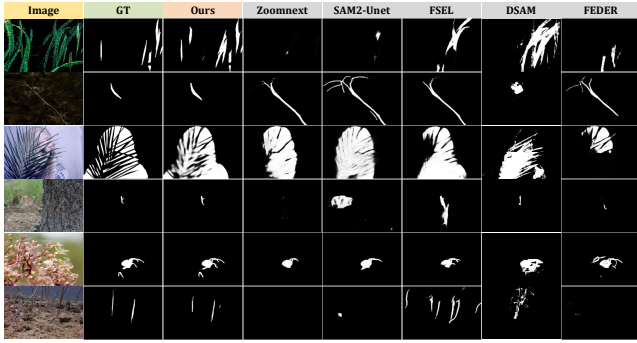


Figure 5: Representative visual results from various methods.

where $\{P_3, P_2, P_1\}$ represent the predictions generated by our decoder and G refers to the ground truth mask.

4 Experiments

4.1 Experimental Settings

Datasets. We train and evaluate the proposed RetroMem on four widely used COD datasets. The training set comprises samples from CAMO [32] and COD10K [12], totaling 4,040 images. For evaluation, we utilize the CAMO, COD10K, NC4K [36] and CHAMELEON [47] datasets, containing 250, 2,026, 4,121, and 76 images, respectively. More details can be found in the [supplementary material](#) (Sec. A.1).

Criteria. To assess model effectiveness, five commonly-used metrics are introduced: S-measure (S_α) [10], E-measure (E_m) [11], weighted F-measure (F_β^ω) [38], adaptive F-measure (F_β) [52], and mean absolute error (M). Higher values for S_α , F_β^ω , F_β and E_m indicate better performance, whereas a lower M signifies improved accuracy. More details about metrics can be found in the [supplementary material](#).

Implementation. The proposed RetroMem is implemented using the PyTorch framework and trained on an NVIDIA RTX 3090 GPU. All experiments adopt a batch size of 12. Input images are resized to 448×448 . We utilize the AdamW [29] optimizer and employ the DINOv2-B/14 [43] as the vision backbone. The proposed dense multi-scale adapter (DMA) is applied at layers $\{1, 3, 5, 7, 9, 11\}$ within the frozen DINOv2. For layer selection, We performed an ablation study on layer selection in the [supplementary material](#) (Section. B.2) to validate the chosen DMA insertion layers.

4.2 Comparison with State-of-the-Art Methods

To evaluate the method effectiveness, we compare RetroMem against several state-of-the-art conventional [13, 18, 24–26, 35, 40, 44, 45, 54–56, 65, 69, 70, 72] and finetuning-based [2, 3, 62, 71] methods, as well as existing RGB-D [60, 66] and vision-text methods [68, 69]. For a fair comparison, all prediction results are obtained directly from the authors’ official implementations.

Quantitative Result. As shown in Tab. 1 and Tab. 2, our RetroMem outperforms all 23 competing methods, except for BiRefNet in F_β^ω on COD10K. Notably, compared to recent COD methods such as BiRefNet, RISNet, ACUMEN, and DSAM, which leverage high-resolution inputs or incorporate additional modalities information (e.g., textual descriptions, depth maps) to enhance performance, our

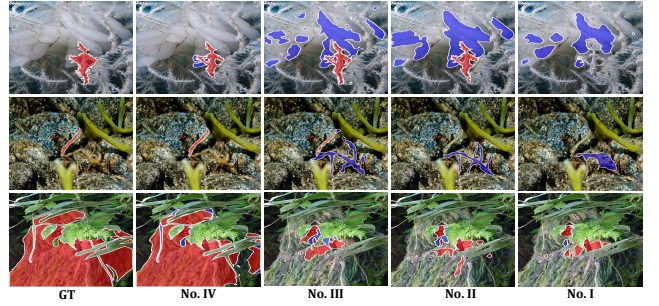


Figure 6: Visual comparison of the variants No. I-IV shown in Tab. 3. The red and blue regions represent correct and error predictions, respectively.

method exhibits strong performance across all benchmark datasets. Specifically, compared to the high-resolution method BiRefNet, our model achieves average improvements of 1.2%, 2.8%, 1.4%, and 15.1% in S_m , F_β^ω , E_m , and M , respectively. Furthermore, although certain finetuning-based methods utilize more complex pre-trained backbones (e.g., ViT-L, ViT-H) to enhance performance, a performance gap still persists in comparison with our approach. In addition, RetroMem surpasses the finetuning-based FGSA-Net [71] by 2.5%, 7.9%, 4.6%, and 18.7% in the same metrics.

Qualitative Result. As illustrated in Fig. 7, most camouflage patterns in the training dataset focus on background matching (e.g., color, shape, texture), while rare cases such as extreme sizes, edge blurring, noise interference, multiple objects, and improper exposure are underrepresented. Thus, we emphasize these challenging scenes in our evaluation. Fig. 5 compares our method with SOTA approaches. For large and small objects (3rd and 4th rows), RetroMem achieves more complete segmentation while preserving contours. In multi-object cases (1st and 6th rows), it accurately detects all objects. Under low-light conditions with noise interference (second row), our memory mechanism recalls relevant camouflage pattern knowledge, enabling correct segmentation where other methods fail. These results highlight the superior generalization capability of RetroMem in complex camouflage scenes. We provide more visual comparisons in the [supplementary material](#) (Sec. C).

4.3 Ablation Study

Effectiveness of DMA. As shown in Tab. 3, the effectiveness of the DMA can be validated by comparing variants No. I and II. Efficient parameter fine-tuning introduces only a small number of trainable parameters while significantly improving model performance. Transitioning from No. I to No. II leads to notable improvements across all evaluation metrics: the M value increases by an average of 52%, the F_β^ω value by 22.1%, the F_β value by 24.3%, and the E_m value by 15.7%. These results demonstrate that the DMA effectively enhances the performance of DINOv2-based models in the COD task. Furthermore, as illustrated in Fig 6, the visual comparison between No. I and II clearly shows that our DMA enables the model to acquire multi-scale information, thereby locating objects more accurately in complex environments. And we compare

Table 1: Quantitative results. Top-three results are highlighted in red, green, and blue. “-” indicates publicly unavailable results.

Methods	Year	Backbone	CAMO (250 images)					COD10K (2,026 images)					NC4K (4,121 images)				
			$S_\alpha \uparrow$	$F_\beta^\omega \uparrow$	$F_\beta \uparrow$	$M \downarrow$	$E_m \uparrow$	$S_\alpha \uparrow$	$F_\beta^\omega \uparrow$	$F_\beta \uparrow$	$M \downarrow$	$E_m \uparrow$	$S_\alpha \uparrow$	$F_\beta^\omega \uparrow$	$F_\beta \uparrow$	$M \downarrow$	$E_m \uparrow$
CNN and Transformer based Methods																	
SINet [13]	CVPR'2020	ResNet [19]	0.751	0.644	0.702	0.100	0.771	0.751	0.551	0.679	0.051	0.806	0.808	0.723	0.769	0.058	0.887
PFNet [40]	CVPR'2021	ResNet [19]	0.782	0.695	0.746	0.085	0.855	0.800	0.660	0.701	0.040	0.877	0.829	0.745	0.784	0.053	0.887
BGNet [55]	IJCAI'2022	Res2Net [15]	0.812	0.749	0.789	0.073	0.870	0.831	0.722	0.753	0.033	0.901	0.851	0.788	0.820	0.044	0.907
ZoomNet [44]	CVPR'2022	ResNet [19]	0.820	0.752	0.794	0.066	0.877	0.838	0.729	0.766	0.029	0.888	0.853	0.784	0.818	0.043	0.896
FEDER [18]	CVPR'2023	Res2Net [15]	0.836	0.807	0.781	0.066	0.897	0.844	0.748	0.751	0.029	0.911	0.862	0.824	0.824	0.042	0.913
FSPNet [26]	CVPR'2023	ViT [8]	0.851	0.802	0.831	0.056	0.905	0.850	0.755	0.769	0.028	0.912	0.879	0.816	0.843	0.035	0.914
HitNet [24]	AAAI'2023	PVT-B2 [61]	0.849	0.809	0.831	0.055	0.906	0.871	0.806	0.823	0.023	0.935	0.875	0.834	0.854	0.037	0.926
PRNet [25]	TCSVT'2024	PVT-B2 [61]	0.872	0.831	0.855	0.050	0.922	0.874	0.799	0.855	0.023	0.937	0.891	0.848	0.869	0.031	0.935
DSAM [66]	MM'2024	SAM [3]	0.825	0.798	0.824	0.061	0.917	0.837	0.766	0.789	0.033	0.925	0.864	0.832	0.851	0.040	0.932
FSEL [56]	ECCV'2024	PVT-B4 [61]	0.885	0.857	0.868	0.040	0.942	0.877	0.799	0.817	0.021	0.937	0.892	0.852	0.871	0.030	0.941
ACUMEN [69]	ECCV'2024	CLIP-L [49]	0.886	0.850	0.861	0.039	0.939	0.852	0.761	0.778	0.026	0.930	0.874	0.826	0.844	0.036	0.932
CamoFormer [65]	TPAMI'2024	PVT-B4 [61]	0.872	0.831	0.854	0.046	0.929	0.869	0.786	0.842	0.023	0.932	0.892	0.847	0.868	0.030	0.939
ZoomNeXt [45]	TPAMI'2024	PVT-B4 [61]	0.888	0.859	0.878	0.040	0.943	0.898	0.838	0.848	0.017	0.955	0.900	0.865	0.884	0.028	0.949
RISNet [60]	CVPR'2024	PVT-B2 [61]	0.870	0.827	0.844	0.050	0.922	0.873	0.799	0.817	0.025	0.931	0.882	0.834	0.854	0.037	0.926
ViCode [35]	CVPR'2024	Swin-T [33]	0.873	0.820	0.844	0.046	0.925	0.869	0.780	0.806	0.025	0.931	0.882	0.841	0.863	0.032	0.935
HGINet [64]	TIP'2024	ViT+RTFA [8]	0.874	0.848	0.868	0.041	0.937	0.882	0.821	0.835	0.019	0.949	0.894	0.865	0.880	0.027	0.947
CGNet [68]	Arxiv'2024	CLIP [49]	0.896	0.864	0.882	0.036	0.947	0.890	0.824	0.859	0.018	0.948	0.904	0.869	0.887	0.026	0.949
BiRefNet [72]	AIR'2024	Swin-L [33]	0.904	0.890	-	0.030	0.954	0.913	0.874	-	0.014	0.960	0.914	0.894	-	0.023	0.953
CamoDiffusion [54]	TPAMI'2025	PVT-B4 [61]	0.878	0.853	-	0.042	0.940	0.881	0.814	-	0.026	0.895	0.893	0.859	-	0.035	0.942
Finetuning-based Methods																	
SAM-Adapter [3]	ICCVW'2023	SAM-H [3]	0.847	0.765	-	0.070	0.873	0.883	0.824	-	0.025	0.918	-	-	-	-	-
FGSA-Net [71]	TMM'2024	ViT-L [8]	0.889	0.870	-	0.036	0.944	0.893	0.849	-	0.015	0.953	0.903	0.883	-	0.023	0.951
SAM2-UNet [62]	Arxiv'2024	SAM2-L [30]	0.884	0.844	0.864	0.042	0.932	0.880	0.789	0.800	0.021	0.936	0.901	0.856	0.872	0.029	0.941
SAM2-Adapter [2]	Arxiv'2024	SAM2-L [30]	0.855	0.810	-	0.051	0.909	0.899	0.850	-	0.018	0.950	-	-	-	-	-
RetroMem	Ours	DINOv2-B [43]	0.913	0.894	0.903	0.028	0.959	0.915	0.868	0.876	0.014	0.966	0.923	0.900	0.910	0.020	0.963

Table 2: Performance on CHAMELEON [47] dataset.

Methods	Year	CHAMELEON (76 images)				
		$S_\alpha \uparrow$	$F_\beta^\omega \uparrow$	$F_\beta \uparrow$	$M \downarrow$	$E_m \uparrow$
SINet [13]	CVPR'2020	0.869	0.740	0.790	0.044	0.899
PFNet [40]	CVPR'2021	0.882	0.810	0.828	0.033	0.942
BGNet [55]	IJCAI'2022	0.901	0.851	0.860	0.027	0.943
ZoomNet [44]	CVPR'2022	0.902	0.845	0.864	0.023	0.952
FEDER [18]	CVPR'2023	0.887	0.834	0.851	0.030	0.946
FSPNet [26]	CVPR'2023	0.908	0.851	0.867	0.022	0.943
HitNet [24]	AAAI'2023	0.921	0.897	0.902	0.019	0.967
PRNet [25]	TCSVT'2024	0.914	0.874	0.886	0.020	0.971
FSEL [56]	ECCV'2024	0.916	0.880	0.889	0.022	0.958
CamoFormer [65]	TPAMI'2024	0.910	0.865	0.882	0.022	0.957
ZoomNeXt [45]	TPAMI'2024	0.924	0.885	0.896	0.018	0.975
RetroMem (Ours)	-	0.931	0.903	0.908	0.017	0.972

our method with four representative fine-tuning approaches, including Series-Adapter [22], Parallel-Adapter [46], LoRA [23], and ViT-Adapter [4]. All methods adopt the same pretrained backbone and initialization weights to ensure a fair comparison. As shown in Tab. 4, RetroMem consistently outperforms all baselines across both COD10K and NC4K benchmarks, achieving the best results in all five evaluation metrics. This demonstrates the superiority of our densely-connected multi-scale design in enhancing camouflaged object perception with minimal computational overhead. We also supplement more ablation studies of the DMA in the [supplementary material](#) (Sec. B.2).

Table 3: Ablation comparison of proposed components. “Param.” means the number of trainable parameters.

No.	Variants	Param. (M)	MACs (G)	FPS	COD10K (2,026 images)					NC4K (4,121 images)				
					$S_\alpha \uparrow$	$F_\beta^\omega \uparrow$	$F_\beta \uparrow$	$M \downarrow$	$E_m \uparrow$	$S_\alpha \uparrow$	$F_\beta^\omega \uparrow$	$F_\beta \uparrow$	$M \downarrow$	$E_m \uparrow$
<i>Stage 1: Learning</i>														
I	Baseline	0.53	27.90	71.81	0.780	0.693	0.702	0.054	0.810	0.722	0.660	0.675	0.065	0.761
II	No. I+DMA	4.98	28.32	62.50	0.881	0.833	0.844	0.023	0.930	0.898	0.846	0.860	0.030	0.941
<i>Stage 2: Recall</i>														
III	No. II+IPR	36.03	38.12	28.89	0.908	0.855	0.864	0.017	0.948	0.914	0.869	0.864	0.025	0.953
IV	No. II+IPR+DMM	40.01	39.84	22.68	0.915	0.868	0.886	0.014	0.966	0.923	0.900	0.910	0.020	0.963
V	No. IV w/o Transformer	36.03	38.73	24.13	0.916	0.855	0.871	0.016	0.957	0.919	0.893	0.902	0.022	0.959
VI	No. IV w/o HDBSCAN	40.01	39.84	12.30	0.912	0.857	0.871	0.017	0.959	0.920	0.892	0.886	0.022	0.960
VII	No. IV w/o \mathcal{L}_c	40.01	39.84	22.68	0.909	0.878	0.886	0.018	0.960	0.920	0.895	0.886	0.021	0.962

Table 4: Comparison of different parameter-efficient fine-tuning methods based on No. II in Tab. 3. All GPU memory values are measured with a batch size of 10.

Methods	GPU Mem (GB)	COD10K (2,026 images)					NC4K (4,121 images)				
		$S_\alpha \uparrow$	$F_\beta^\omega \uparrow$	$F_\beta \uparrow$	$M \downarrow$	$E_m \uparrow$	$S_\alpha \uparrow$	$F_\beta^\omega \uparrow$	$F_\beta \uparrow$	$M \downarrow$	$E_m \uparrow$
Full-Tuning	18G	0.872	0.822	0.833	0.026	0.925	0.889	0.836	0.849	0.031	0.935
Frozen-Backbone	1G	0.780	0.693	0.702	0.054	0.810	0.722	0.660	0.675	0.065	0.761
Series-Adapter [22]	4G	0.840	0.756	0.771	0.026	0.874	0.835	0.780	0.792	0.036	0.875
Parallel-Adapter [46]	4G	0.847	0.763	0.776	0.025	0.880	0.855	0.801	0.810	0.034	0.894
ViT-Adapter [4]	4G	0.863	0.777	0.790	0.025	0.895	0.878	0.825	0.835	0.033	0.917
LoRA [23]	2G	0.831	0.746	0.756	0.028	0.865	0.812	0.755	0.770	0.037	0.854
DMA (Ours)	3G	0.881	0.833	0.844	0.023	0.930	0.898	0.848	0.860	0.030	0.941

Effectiveness of IPR. The variant No. III extends the learning stage model (No. II) by incorporating the IPR. This enhancement leads to average performance gains of 13.5% and 8.75% on COD10K and NC4K, respectively, when transitioning from No. II to No. III. These improvements indicate that No. III enhances the semantic

Table 5: Ablation comparison of clustering algorithm.

Settings	FPS	COD10K (2,026 images)					NC4K (4,121 images)				
		$S_a \uparrow$	$F_{\beta}^o \uparrow$	$F_{\beta} \uparrow$	$M \downarrow$	$E_m \uparrow$	$S_a \uparrow$	$F_{\beta}^o \uparrow$	$F_{\beta} \uparrow$	$M \downarrow$	$E_m \uparrow$
Direct Match	12.30	0.906	0.857	0.868	0.017	0.952	0.911	0.882	0.893	0.024	0.960
K-Means	30.63	0.902	0.847	0.862	0.016	0.949	0.914	0.874	0.883	0.023	0.953
DBSCAN	24.12	0.910	0.862	0.871	0.015	0.958	0.917	0.893	0.902	0.021	0.957
HDBSCAN	22.68	0.915	0.868	0.886	0.014	0.966	0.923	0.900	0.910	0.020	0.963

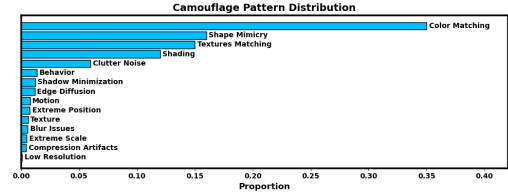
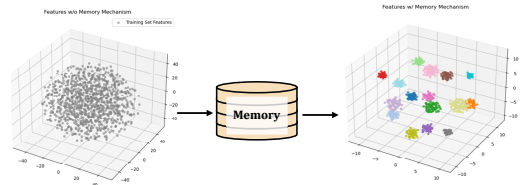
perception capabilities for camouflaged objects in most scenes. Despite these advancements, no DMM is incorporated to complement the IPR, which functions solely as a feature fusion module. Consequently, the inference capabilities of RetroMem are not fully developed. This limitation is evident in the visual results of No. III shown in Fig. 6, where the model fails to detect camouflaged objects. The observation indicates that No. III lacks sufficient generalization ability in challenging camouflage scenes.

Effectiveness of DMM. We validate the effectiveness of our memory mechanism (DMM) through both visualization (Fig. 6) and quantitative comparisons (Tab. 3). The variant No. IV demonstrates superior localization accuracy and noise suppression compared to the baseline variant. This improvement is achieved through the IPR’s reconstruction of sample-adaptive inference patterns that strategically utilize knowledge from the memory mechanism. The collaboration of the IPR and the DMM significantly improves the model’s capability to handle both unseen and rarely encountered camouflage scenes. Moreover, the results of No. V and No. VI in Tab. 3 further demonstrate the superiority of our memory mechanism design. Specifically, in No. VI, we remove HDBSCAN [39] and the prototype computation process, opting instead to memory mechanism by computing the similarity between each training sample and the current sample. Compared to No. IV, No. VI suffers a 50% decrease in inference speed, and the memory storage increases from 150 KB to 8 MB (90% increase), accompanied by an average performance drop of 6.25%. In more detail, we visualize the features before and after the dynamic memory mechanism through t-SNE, as shown in Fig. 8. We also provide more analysis on the memory in the [supplementary material](#) (Sec. B.3).

Selection of Clustering Algorithm. To evaluate the role of clustering algorithms in the DMM, we compare three popular algorithms in Tab. 5: K-Means [37], DBSCAN [9], and HDBSCAN [39], along with a simple “Direct Match” baseline that computes similarity without clustering. Since K-Means requires a pre-defined number of clusters, it becomes less suitable for COD, where object classes are highly diverse and not explicitly annotated. To address this, we approximate the number of camouflaged object classes in the training set and set the number of clusters to 103 accordingly. Experiments on COD benchmarks reveal that HDBSCAN delivers superior performance and more stable clustering, while Direct Match and K-Means lags due to its lack of adaptive refinement. Compared to Direct Match, centralized matching (e.g., HDBSCAN, DBSCAN, K-Means) significantly reduces inference cost by compressing the recall space into a small set of representative prototypes. Consequently, we select HDBSCAN as the clustering module for generating compact and discriminative memory representations.

Table 6: Comparison on challenging camouflage scenes.

Methods	Seen Scenes (6,109 images)					Unseen Scenes (364 images)					Rare Scenes (91 images)				
	$S_a \uparrow$	$F_{\beta}^o \uparrow$	$F_{\beta} \uparrow$	$M \downarrow$	$E_m \uparrow$	$S_a \uparrow$	$F_{\beta}^o \uparrow$	$F_{\beta} \uparrow$	$M \downarrow$	$E_m \uparrow$	$S_a \uparrow$	$F_{\beta}^o \uparrow$	$F_{\beta} \uparrow$	$M \downarrow$	$E_m \uparrow$
SINet [13]	0.797	0.693	0.703	0.054	0.868	0.786	0.680	0.690	0.051	0.858	0.477	0.095	0.096	0.107	0.588
PFNet [40]	0.820	0.719	0.730	0.050	0.884	0.801	0.694	0.705	0.051	0.868	0.485	0.128	0.130	0.121	0.586
BGNet [55]	0.845	0.768	0.780	0.042	0.905	0.827	0.741	0.752	0.043	0.873	0.512	0.164	0.167	0.111	0.581
ZoomNet [44]	0.849	0.768	0.780	0.039	0.894	0.826	0.733	0.744	0.043	0.875	0.522	0.176	0.179	0.095	0.608
FEDER [18]	0.840	0.767	0.779	0.041	0.905	0.813	0.725	0.736	0.045	0.873	0.522	0.193	0.196	0.098	0.630
HitNet [24]	0.875	0.827	0.840	0.033	0.929	0.856	0.797	0.809	0.035	0.916	0.575	0.284	0.288	0.103	0.678
RISNet [60]	0.880	0.825	0.838	0.033	0.928	0.860	0.794	0.806	0.038	0.910	0.571	0.273	0.277	0.112	0.620
FSEL [56]	0.889	0.838	0.851	0.027	0.943	0.867	0.807	0.819	0.032	0.921	0.593	0.314	0.319	0.090	0.665
CGNet [68]	0.900	0.854	0.867	0.024	0.954	0.882	0.819	0.831	0.029	0.926	0.630	0.356	0.361	0.073	0.715
RetroMem	0.918	0.888	0.901	0.019	0.964	0.901	0.858	0.871	0.022	0.942	0.733	0.540	0.548	0.042	0.815

**Figure 7: Camouflage pattern distribution of training data.****Figure 8: Details of the t-SNE method.**

Generalization Ability. To evaluate the generalization ability of COD methods, we categorize all data from image COD testing sets including CAMO, COD10K, NC4K, and CHAMELEON, and several representative samples from the video COD dataset MoCA-Mask [6] into seen, unseen, and rare scenes. As shown in Fig. 7, samples with camouflage patterns whose training samples account for less than 5% of the total training set are identified as rare scenes. Unseen scenes contain samples that do not include any object classes present in the training set. This facilitates a more comprehensive evaluation for model generalization and robustness in challenging real-world scenes. As shown in Tab. 6, RetroMem consistently outperforms all comparison methods on these datasets. Compared with the latest SOTA method, CGNet [68], our network achieves performance gains of 7%, 10% and 31% on these three sets, with an even more significant improvement in the rare scene. This advantage primarily stems from the synergy between our IPR and DMM, allowing the model to incorporate historical information and reconstruct an adaptive inference pattern for each sample. Consequently, the proposed RetroMem exhibits stronger generalization ability in challenging camouflage scenes.

5 Conclusion

We propose **RetroMem**, a novel two-stage COD framework comprising a learning stage and a recall stage. By the collaboration of these two stages, the system establishes a context-aware inference mechanism capable of maintaining robust performance

across diverse camouflage scenes. RetroMem alleviates the existing limitations of static inference patterns and reliance on instantaneous visual features through the synergistic integration of sample representations and recalled historical knowledge. Extensive experiments conducted on the widely-used conventional COD datasets and carefully-constructed challenging benchmarks demonstrate that our RetroMem achieves superior performance compared to other state-of-the-art methods.

References

- [1] David G T Barrett, Ari S Morcos, and Jakob H Macke. 2019. Analyzing biological and artificial neural networks: challenges with opportunities for synergy? *Current Opinion in Neurobiology* 55 (2019), 55–64.
- [2] Tianrun Chen, Ankang Lu, Lanyun Zhu, Chaotao Ding, Chunan Yu, Deyi Ji, Zejian Li, Lingyun Sun, Papa Mao, and Ying Zang. 2024. Sam2-adapter: Evaluating & adapting segment anything 2 in downstream tasks: Camouflage, shadow, medical image segmentation, and more. *arXiv preprint arXiv:2408.04579* (2024).
- [3] T. Chen, L. Zhu, C. Deng, R. Cao, Y. Wang, S. Zhang, Z. Li, and P. Sun. 2023. SAM-Adapter: Adapting Segment Anything in Underperformed Scenes. In *ICCVW*.
- [4] Yuhang Chen, Jianan Wang, Jie Zhou, Qian Yu, Jifeng Dai, and Tong Lu. 2023. Vision Transformer Adapter for Dense Predictions. In *ICLR*.
- [5] Seoung Wug Cheng, Jang Hyun Park, and Donggeun Yoo. 2022. XMem: Long-term video object segmentation with an online memory module. In *NeurIPS*.
- [6] Xuelian Cheng, Huan Xiong, Deng-Ping Fan, Yiran Zhong, Mehrtash Harandi, Tom Drummond, and Zongyuan Ge. 2022. Implicit motion handling for video camouflaged object detection. In *CVPR*. 13864–13873.
- [7] Thomas M Cover and Peter E Hart. 1967. Nearest neighbor pattern classification. *IEEE Transactions on Information Theory* 13, 1 (1967), 21–27.
- [8] Alexey Dosovitskiy, Lucas Beyer, Alexander Kolesnikov, Dirk Weissenborn, Xi-aohua Zhai, Thomas Unterthiner, Mostafa Dehghani, Matthias Minderer, Georg Heigold, Sylvain Gelly, Jakob Uszkoreit, and Neil Houlsby. 2021. An Image is Worth 16x16 Words: Transformers for Image Recognition at Scale. In *ICLR*. <https://openreview.net/forum?id=YicbFdNTTy>
- [9] Martin Ester, Hans-Peter Kriegel, Jörg Sander, and Xiaowei Xu. 1996. A density-based algorithm for discovering clusters in large spatial databases with noise. In *KDD*. AAAI Press, 226–231.
- [10] D Fan, M Cheng, Y Liu, T Li, and A Botji. 2017. Structure-measure: A new way to evaluate foreground maps. In *Proc. IEEE/CVF Int. Conf. Comput. Vis.* 4548–4557.
- [11] Deng-Ping Fan, Cheng Gong, Yang Cao, Bo Ren, Ming-Ming Cheng, and Ali Borji. 2018. Enhanced-alignment Measure for Binary Foreground Map Evaluation. In *In IJCAL*. 698–704.
- [12] Deng-Ping Fan, Ge-Peng Ji, Ming-Ming Cheng, and Ling Shao. 2022. Concealed Object Detection. *TPAMI* 44, 10 (2022), 6024–6042.
- [13] Deng-Ping Fan, Ge-Peng Ji, Guolei Sun, Ming-Ming Cheng, Jianbing Shen, and Ling Shao. 2020. Camouflaged Object Detection. In *CVPR*. 2774–2784.
- [14] Deng-Ping Fan, Ge-Peng Ji, Tao Zhou, Geng Chen, Huazhu Fu, Jianbing Shen, and Ling Shao. 2020. Pranet: Parallel reverse attention network for polyp segmentation. In *International conference on medical image computing and computer-assisted intervention*. Springer, 263–273.
- [15] Shang-Hua Gao, Ming-Ming Cheng, Kai Zhao, Xin-Yu Zhang, Ming-Hsuan Yang, and Philip Torr. 2021. Res2Net: A New Multi-Scale Backbone Architecture. *TPAMI* 43, 2 (2021), 652–662.
- [16] Dong Gong, Lingqiao Liu, Vuong Le, Budhaditya Saha, Moussa Reda Mansour, Svetha Venkatesh, and Anton van den Hengel. 2019. Memorizing normality to detect anomaly: Memory-augmented deep autoencoder for unsupervised anomaly detection. In *ICCV*. 1705–1714.
- [17] Demis Hassabis, Dharshan Kumaran, Christopher Summerfield, and Matthew Botvinick. 2017. Neuroscience-inspired artificial intelligence. *Neuron* 95, 2 (2017), 245–258.
- [18] Chunming He, Kai Li, Yachao Zhang, Longxiang Tang, Yulun Zhang, Zhenhua Guo, and Xiu Li. 2023. Camouflaged Object Detection with Feature Decomposition and Edge Reconstruction. In *CVPR*. 22046–22055.
- [19] Kaiming He, Xiangyu Zhang, Shaoqing Ren, and Jian Sun. 2016. Deep residual learning for image recognition. In *Proc. IEEE/CVF Int. Conf. Comput. Vis.* 770–778.
- [20] Sepp Hochreiter and Jürgen Schmidhuber. 1997. Long short-term memory. *Neural computation* 9, 8 (1997), 1735–1780.
- [21] Jianqin Yin Yanbin Han Wendi Hou and Jinping Li. 2011. Detection of the mobile object with camouflage color under dynamic background based on optical flow. *Procedia Engineering* 15 (2011), 2201–2205.
- [22] Neil Houlsby, Andrei Giurgiu, Stanislaw Jastrzebski, and et al. 2019. Parameter-efficient transfer learning for NLP. In *ICML*.
- [23] Edward Hu, Yelong Shen, Phil Wallis, Zeyuan Allen-Zhu, Yuanzhi Li, Lu Wang, and Weizhu Chen. 2021. LoRA: Low-Rank Adaptation of Large Language Models. *arXiv preprint arXiv:2106.09685* (2021).
- [24] Xiaobin Hu, Shuo Wang, Xuebin Qin, Hang Dai, Wenqi Ren, Donghao Luo, Ying Tai, and Ling Shao. 2023. High-resolution iterative feedback network for camouflaged object detection. In *Proceedings of the AAAI*, Vol. 37. 881–889.
- [25] Xihang Hu, Xiaoli Zhang, Fasheng Wang, Jing Sun, and Fuming Sun. 2024. Efficient Camouflaged Object Detection Network Based on Global Localization Perception and Local Guidance Refinement. *TCSVT* 34, 7 (2024), 5452–5465.
- [26] Zhou Huang, Hang Dai, Tian-Zhu Xiang, Shuo Wang, Huai-Xin Chen, Jie Qin, and Huan Xiong. 2023. Feature Shrinkage Pyramid for Camouflaged Object Detection with Transformers. In *CVPR*. 5557–5566.
- [27] Xi Jiang, Jianlin Liu, Jinbao Wang, Qiang Nie, Kai Wu, Yong Liu, Chengjie Wang, and Feng Zheng. 2022. SoftPatch: Unsupervised anomaly detection with noisy data. In *NeurIPS*, Vol. 35. 15433–15445.
- [28] Hyunwoo Jung et al. 2025. TailedCore: Few-Shot Sampling for Unsupervised Long-Tail Noisy Anomaly Detection. *CVPR* (2025).
- [29] Diederik P Kingma. 2014. Adam: A method for stochastic optimization. *arXiv preprint arXiv:1412.6980* (2014).
- [30] Alexander Kirillov, Eric Tzeng, Shubham Tulsiani, Golnaz Ghiasi, Rui Zhu, Xi-aowei Hu, Wentao Liu, Deva Ramanan, Alexander C. Berg, Piotr Dollár, and Ross Girshick. 2024. Segment Anything v2: Scaling Masked Image Pretraining for Localization. *arXiv preprint arXiv:2404.07143* (2024). <https://arxiv.org/abs/2404.07143>
- [31] Brenden M Lake, Tomer D Ullman, Joshua B Tenenbaum, and Samuel J Gershman. 2017. Building machines that learn and think like people. *Behavioral and Brain Sciences* 40 (2017), e253.
- [32] Trung-Nghia Le, Tam V. Nguyen, Zhongliang Nie, Minh-Triet Tran, and Akihiro Sugimoto. 2019. Anabranch network for camouflaged object segmentation. *CVIU* 184 (2019), 45–56.
- [33] Ze Liu, Yutong Lin, Yuqi Cao, Han Hu, Yixuan Wei, Zheng Zhang, Stephen Lin, and Baining Guo. 2021. Swin Transformer: Hierarchical Vision Transformer using Shifted Windows. In *ICCV*. 10012–10022.
- [34] Jiannan Lu, Zenglin Lu, and Yi Yang. 2020. Video object segmentation with episodic graph memory networks. In *ECCV*.
- [35] Ziyang Luo, Nian Liu, Wangbo Zhao, Xuguang Yang, Dingwen Zhang, Deng-Ping Fan, Fahad Khan, and Junwei Han. 2024. VSCoDe: General Visual Salient and Camouflaged Object Detection with 2D Prompt Learning. In *CVPR*. 17169–17180.
- [36] Yunqiu Lv, Jing Zhang, Yuchao Dai, Aixuan Li, Bowen Liu, Nick Barnes, and Deng-Ping Fan. 2021. Simultaneously Localize, Segment and Rank the Camouflaged Objects. In *CVPR*. 11586–11596.
- [37] J. MacQueen. 1967. Some methods for classification and analysis of multivariate observations. In *Proceedings of the Fifth Berkeley Symposium on Mathematical Statistics and Probability, Volume 1: Statistics*. University of California Press, 281–297.
- [38] R. Margolin, L. Zelnik-Manor, and A. Tal. 2014. How to evaluate foreground maps. In *CVPR*. 248–255.
- [39] Leland McInnes, John Healy, Steve Astels, et al. 2017. hdbscan: Hierarchical density based clustering. *J. Open Source Softw.* 2, 11 (2017), 205.
- [40] Haiyang Mei, Ge-Peng Ji, Ziqi Wei, Xin Yang, Xiaopeng Wei, and Deng-Ping Fan. 2021. Camouflaged Object Segmentation with Distraction Mining. In *CVPR*. 8768–8777.
- [41] Melia G Nafus, Jennifer M Germano, Jeanette A Perry, Brian D Todd, Allyson Walsh, and Ronald R Swaisgood. 2015. Hiding in plain sight: a study on camouflage and habitat selection in a slow-moving desert herbivore. *Behavioral Ecology* 26, 5 (2015), 1389–1394.
- [42] Seoung Wug Oh, Joon-Young Lee, Ning Xu, and Seon Joo Kim. 2019. Video object segmentation using space-time memory networks. In *ICCV*. 9226–9235.
- [43] Maxime Oquab, Timothée Darcet, Théo Moutakanni, Huy Vo, Marc Szafraniec, Vasil Khalidov, Pierre Fernandez, Daniel Haziza, Francisco Massa, Alaaeldin El-Nouby, Mahmoud Assran, Nicolas Ballas, Wojciech Galuba, Russell Howes, Po-Yao Huang, Shang-Wen Li, Ishan Misra, Michael Rabbat, Vasu Sharma, Gabriel Synnaeve, Hu Xu, Hervé Jegou, Julien Mairal, Patrick Labatut, Armand Joulin, and Piotr Bojanowski. 2023. DINOv2: Learning Robust Visual Features without Supervision. *arXiv preprint arXiv:2304.07193* (2023).
- [44] Youwei Pang, Xiaoqi Zhao, Tian-Zhu Xiang, Lihe Zhang, and Huchuan Lu. 2022. Zoom in and Out: A Mixed-Scale Triplet Network for Camouflaged Object Detection. In *CVPR*. 2160–2170.
- [45] Youwei Pang, Xiaoqi Zhao, Tian-Zhu Xiang, Lihe Zhang, and Huchuan Lu. 2024. ZoomNeXt: A Unified Collaborative Pyramid Network for Camouflaged Object Detection. *TPAMI* (2024). doi:10.1109/TPAMI.2024.3417329
- [46] Jonas Pfeiffer, Ameya Kamath, Sebastian Ruder, and Iryna Gurevych. 2021. AdapterFusion: Non-Destructive Task Composition for Transfer Learning. In *EACL*.
- [47] Skurowski Przemyslaw, Abdulameer Hassan, Błaszczak Jakub, Depta Tomasz, Kornacki Adam, and Przemyslaw Koziel. 2018. Animal camouflage analysis: Chameleon database. *Unpublished Manuscript* (2018).
- [48] Chennamsetty Pulla Rao, A Guruva Reddy, and CB Rama Rao. 2020. Camouflaged object detection for machine vision applications. *International Journal of Speech Technology* 23 (2020), 327–335.

- [49] Alec Radford, Jong Wook Kim, Chris Hallacy, Aditya Ramesh, Gabriel Goh, Sandhini Agarwal, Girish Sastry, Amanda Askell, Pamela Mishkin, Jack Clark, et al. 2021. Learning transferable visual models from natural language supervision. In *ICML*. PMLR, 8748–8763.
- [50] Karsten Roth, Latha Pemula, Joaquin Zepeda, Bernhard Schölkopf, Thomas Brox, and Peter Gehler. 2022. Towards total recall in industrial anomaly detection. In *CVPR*. 14318–14328.
- [51] Dan Jeric Arcega Rustia, Chien Erh Lin, Jui-Yung Chung, Yi-Ji Zhuang, Ju-Chun Hsu, and Ta-Te Lin. 2020. Application of an image and environmental sensor network for automated greenhouse insect pest monitoring. *Journal of Asia-Pacific Entomology* 23, 1 (2020), 17–28.
- [52] A. Salvador and C. Sminchisescu. 2011. Superpixel-based segmentation evaluation: Adaptive F-measure. In *CVPR*. IEEE, 3061–3068.
- [53] P. Sengottuvelan, Amitabh Wah, and A. Shanmugam. 2008. Performance of Decamouflaging Through Exploratory Image Analysis. In *Proceedings of International Conference on Emerging Trends in Engineering and Technology*. 6–10.
- [54] Ke Sun, Zhongxi Chen, Xianming Lin, Xiaoshuai Sun, Hong Liu, and Rongrong Ji. 2025. Conditional Diffusion Models for Camouflaged and Salient Object Detection. *TPAMI* (2025).
- [55] Yujia Sun, Shuo Wang, Chenglizhao Chen, and Tian-Zhu Xiang. 2022. Boundary-Guided Camouflaged Object Detection. In *Proc. Int. Joint Conf. Artif. Intell.* 1335–1341.
- [56] Yanguang Sun, Chunyan Xu, Jian Yang, Hanyu Xuan, and Lei Luo. 2024. Frequency-Spatial Entanglement Learning for Camouflaged Object Detection. In *ECCV*. 343–360.
- [57] A Vaswani. 2017. Attention is all you need. *Adv. Neural Inf. Process. Syst.* (2017).
- [58] Kaia L. Vilberg and Michael D Rugg. 2008. Memory retrieval and the parietal cortex: a review of evidence from a dual-process perspective. *Neuropsychologia* 46, 7 (2008), 1787–1799. doi:10.1016/j.neuropsychologia.2008.01.004
- [59] Paul Voigtlaender, Joerg Luiten, Philip HS Torr, and Bastian Leibe. 2019. FEELVOS: Fast End-to-End Embedding Learning for Video Object Segmentation. In *CVPR*. 9481–9490.
- [60] Liqiong Wang, Jinyu Yang, Yanfu Zhang, Fangyi Wang, and Feng Zheng. 2024. Depth-Aware Concealed Crop Detection in Dense Agricultural Scenes. In *CVPR*. 17201–17211.
- [61] Wenhai Wang, Enze Xie, Xiang Li, Deng-Ping Fan, Kaitao Song, Ding Liang, Tong Lu, Ping Luo, and Ling Shao. 2021. Pyramid vision transformer: A versatile backbone for dense prediction without convolutions. In *ICCV*. 568–578.
- [62] Xinyu Xiong, Zihuang Wu, Shuangyi Tan, Wenxue Li, Feilong Tang, Ying Chen, Siying Li, Jie Ma, and Guanbin Li. 2024. SAM2-UNet: Segment Anything 2 Makes Strong Encoder for Natural and Medical Image Segmentation. *arXiv preprint arXiv:2408.08870* (2024). <https://arxiv.org/abs/2408.08870>
- [63] Linjie Yang, Yuchen Fan, and Ning Xu. 2021. Associating objects with memories for open-world video object segmentation. In *NeurIPS*.
- [64] Siyuan Yao, Hao Sun, Tian-Zhu Xiang, Xiao Wang, and Xiaochun Cao. 2024. Hierarchical Graph Interaction Transformer with Dynamic Token Clustering for Camouflaged Object Detection. *arXiv preprint arXiv:2408.15020* (2024).
- [65] Bowen Yin, Xuying Zhang, Deng-Ping Fan, Shaohui Jiao, Ming-Ming Cheng, Luc Van Gool, and Qibin Hou. 2024. Camoformer: Masked separable attention for camouflaged object detection. *TPAMI* (2024).
- [66] Zhenni Yu, Xiaoqin Zhang, LiZhao, Yi Bin, and Guobao Xiao. 2024. Exploring Deeper! Segment Anything Model with Depth Perception for Camouflaged Object Detection. In *ACM Multimedia 2024*. <https://openreview.net/forum?id=d4A0Cw1gVS>
- [67] Chenxi Zhang, Qing Zhang, and Jiayun Wu. 2025. Rethinking Camouflaged Object Detection via Foreground-Background Interactive Learning. In *ICASSP 2025-2025 IEEE International Conference on Acoustics, Speech and Signal Processing (ICASSP)*. IEEE, 1–5.
- [68] Chenxi Zhang, Qing Zhang, Jiayun Wu, and Youwei Pang. 2024. CGCOD: Class-Guided Camouflaged Object Detection. *arXiv preprint arXiv:2412.18977* (2024).
- [69] Hong Zhang, Yixuan Lyu, Qian Yu, Hanyang Liu, Huimin Ma, Ding Yuan, and Yifan Yang. 2025. Unlocking Attributes' Contribution to Successful Camouflage: A Combined Textual and Visual Analysis Strategy. In *Computer Vision – ECCV*. Springer Nature Switzerland, Cham, 315–331.
- [70] Jin Zhang, Ruiheng Zhang, Yanjiao Shi, Zhe Cao, Nian Liu, and Fahad Shahbaz Khan. 2024. Learning Camouflaged Object Detection from Noisy Pseudo Label. In *ECCV*. Springer, 158–174.
- [71] Shizhou Zhang, Dexuan Kong, Yinghui Xing, Yue Lu, Lingyan Ran, Guoqiang Liang, Hexu Wang, and Yanning Zhang. 2024. Frequency-Guided Spatial Adaptation for Camouflaged Object Detection. *TMM* 26, 5 (2024), 1234–1245. doi:10.1109/TMM.2024.1234567
- [72] Peng Zheng, Dehong Gao, Deng-Ping Fan, Li Liu, Jorma Laaksonen, Wanli Ouyang, and Nicu Sebe. 2024. Bilateral Reference for High-Resolution Dichotomous Image Segmentation. *CAAI Artificial Intelligence Research* 3 (2024), 9150038.